

A Numerical Study of Normal Modes of Rotating Neutron Star Models by the Cowling Approximation

Shin'ichirou Yoshida and Yoshiharu Eriguchi

*Department of Earth Science and Astronomy, Graduate School of Arts and Sciences, University of Tokyo,
Komaba, Meguro-ku, Tokyo 153-8902, Japan*

ABSTRACT

A numerical method of mode analysis of rapidly rotating relativistic stellar models by the Cowling approximation is applied to rotating neutron stars with realistic equations of state. For selected equations of state, eigenvalues and eigenfunctions of f-modes are numerically solved for stellar models from non-rotating to maximally rotating states.

Neutral points of the lower order f-modes are determined as a function of the stellar rotational frequency. As in the polytropic case, we find that the bar mode can have neutral points for models with relatively strong gravity. The rotational frequency at the neutral point increases as the gravitational mass of the model becomes larger.

As astrophysical applications of our analysis, we discuss the time scales of gravitational radiation induced instability and the possibility of the resonant excitation of f-modes during inspiraling motion of compact binary systems.

Subject headings: stars:neutron — stars:oscillation — stars:rotation

1. Introduction

In the previous paper (Yoshida & Eriguchi 1997, hereafter YE), we determined neutral stability points of the *Chandrasekhar-Friedman-Schutz* (CFS) instability of general relativistic rotating polytropes, by which non-axisymmetric oscillations of rotating stars are excited through the coupling with gravitational radiation (see Chandrasekhar 1970, Friedman & Schutz 1978, Friedman 1978). In the absence of viscosity this instability sets in at the points where eigenfrequencies of the modes vanish as seen from the inertial observer at spatial infinity. Thus to determine the points on equilibrium sequences of rotating stars where the model begins to become unstable, zero frequency modes in the asymptotically inertial frame must be found.

In YE the equations of state (EOS) of stellar matter were restricted to the simple relation of polytropes and neutral points of the counter-rotating f-modes were obtained. Here the counter-rotating modes denote the oscillations whose phase propagation is retrograde with respect to the stellar rotation as seen from the observer rotating with the star.

In this paper we investigate oscillation modes and their neutral points of stability for more realistic EOS proposed for the neutron star matter. The investigated modes are the same ones as in YE which may be the most susceptible *spheroidal* modes to the CFS instability.¹

It has been discussed that modes with the azimuthal quantum number $m = 3$ to 5, by which the eigenfunction of the modes are decomposed to harmonics having angular φ -coordinate dependence $\sim e^{im\varphi}$, are the most interesting for this instability (Lindblom 1986). Also interesting is the recently discovered bar mode neutral points for rather soft EOS, which never appear in the Newtonian framework (for fully general relativistic treatments, see Stergioulas & Friedman 1997; also see YE). Thus we will investigate these lower order modes in this paper.

Concerning the neutral points to the CFS instability, Morsink et al. (1998, hereafter MSB) investigated realistic neutron star models by applying the numerical method to find the exact neutral modes of general relativistic rotating stars developed by Ster-

gioulas and Friedman (1997). They obtained f-mode neutral points for models with various masses for several representative EOS. Therefore we will compare our results with theirs.

The counter-rotating f-modes are not only interesting in the context of the CFS instability of a single neutron star, but also may play an important role in compact binary systems because they may couple strongly with the tidal potential of the companion. The most significant effect will be the resonant excitation of the modes by the tidal force and its back reaction to the orbital motion of the binary system. We will study this subject in the last section of this paper.

2. Brief Summary of the Solving Method

2.1. Assumptions

We assume that axisymmetric equilibrium stars are rotating uniformly and that the stellar matter is described by zero temperature EOS. Under these assumptions, equilibrium states of relativistic rotating stars are obtained numerically by the KEH scheme (Komatsu et al. 1989). Linear adiabatic perturbations may be a good approximation in the present situation, and it is also assumed that the adiabatic index γ of the perturbation coincides with the local adiabatic index of the equilibrium star as follows:

$$\frac{\epsilon + p}{p} \frac{\Delta p}{\Delta \epsilon} \equiv \gamma = \frac{\epsilon + p}{p} \left(\frac{dp}{d\epsilon} \right)_{E_{\text{quil}}}, \quad (1)$$

where Δ means the Lagrangian perturbation of the corresponding variable. Eulerian perturbations of the metric components are totally omitted as in the previous study (YE), i.e., the Cowling approximation is adopted.

2.2. Equations of State

There exist many candidates for EOS of real neutron stars with zero temperature. We here examine some of the representative EOS to cover the wide range of stiffness.² Our choices are those of 1) Pandharipande with hyperon (denoted by EOS B in Arnett & Bowers 1977), 2) Bethe-Johnson without hyperon (Bethe & Johnson 1974), 3) Bethe-Johnson (EOS C in

¹Recent discovery of the CFS instability of the r-mode and its strong effect on the stellar rotational evolution are also interesting subjects (Andersson 1998, Andersson et al. 1998, Lindblom et al. 1998), but they are beyond the scope of this paper.

²See Nozawa et al. (1998) for recent calculation and summary of equilibrium models with various realistic candidates of cold EOS.

Arnett & Bowers) and 4) more recent WFF3 (Wiringa et al. 1988) joined to NV (Negel & Vautherin 1973) in the low density region. In order to compare our result with those of MSB, the EOS of Pandharipande without hyperon (EOS A in Arnett & Bowers) is also employed. Extremely stiff EOS L in Arnett & Bowers is used only in Figure 8 for the comparison of the EOSs with a wide range of stiffness.

2.3. Numerical Treatment

Our numerical scheme is basically the same as that in YE. Perturbed quantities are assumed to behave as $\sim e^{-2\pi i \nu t + i m \varphi}$, where t is the killing time coordinate. A minor change that has been made is the introduction of a function $q \equiv \delta p / (\epsilon + p)$, instead of the Eulerian perturbation of the Emden function for polytropic stars. Coefficients of the perturbed equations contain the background metric and its connection coefficients as well as the pressure gradient and a function of adiabatic index like $\gamma p / (\epsilon + p)$.³

We have used $(r \times \theta) = (100 \times 61)$ grid points for equilibrium models where (r, θ) are the spherical polar coordinates. Since less number of grid point is used for the perturbational calculation due to the restrictions of the power of the computer, values for equilibrium states are interpolated to give values at the coarse grid points of our surface-fitted coordinate (see YE). The interpolation is done by employing the cubic spline scheme in two dimensions. The results in this paper are obtained by using $(r \times \theta) = (25 \times 12)$ grid points in the surface-fitted coordinate.

3. Results

3.1. Eigenfrequencies and Eigenfunctions

Rotational sequences of equilibrium stars can be obtained by fixing the central energy density ϵ_c and changing the rotational parameter such as the ratio of the polar radius to the equatorial radius in the meridional cross section of the star. Physical quantities such as the gravitational mass, the $T/|W|$ value and the angular momentum, etc. are calculated after equilibrium configurations are computed. Here T and W are the rotational energy and the gravitational energy, respectively, whose definitions can be found in Komatsu et al. (1989) and its ratio can be considered

to be a standard indicator of the stellar rotation. By changing the central density many sequences of equilibrium stars are obtained and a series of models with the same gravitational mass and a different rotational frequency can be chosen. For these equilibrium models the eigenproblem is solved numerically.

In this paper we will concentrate only on the counter-rotating f-modes. They are the generalization of the Kelvin modes of Newtonian Maclaurin spheroids with the counter-rotating phase velocity as seen from the co-rotating observer with the star and have indices $l = m$ of the spheroidal harmonics. These particular modes may be the most susceptible to the CFS instability (see Baumgart & Friedman 1986) and have been mainly investigated as to this instability.

Figures 1 – 7 show the dependency of eigenfrequency ν on the rotational frequency f for the specified EOS and for the fixed gravitational mass. For slowly rotating models, the frequency becomes higher as m increases. Note that, since we are considering the behavior of the perturbed quantities expressed as $\sim e^{-2\pi i \nu t + i m \varphi}$, the phase velocity $2\pi \nu / m$ is negative in this case. As the rotational frequency is increased, the rotational dragging effect on the mode (*not* the ‘inertial-frame-dragging’ effect in general relativity) works more strongly for the larger m modes and the order of the mode frequencies are reversed. As a result, modes with larger m pass the neutral points earlier on the sequences.

Near the mass-shedding limit, eigenvalues rise sharply with the increase of the rotational parameter. By using more detailed data set from which these graphs are produced, we can have much smoother eigenfrequency curves with the fixed central energy density and show that this behavior is also seen there. However, the eigenfunctions of these models show sharp rises of the amplitudes near the surface region on the equatorial plane. Therefore, the rather coarse angular resolution may prevent us from solving the numerical eigenvalue problem accurately near the mass-shedding limit.

Next we show the typical behaviors of the eigenfrequencies of the mode of our interest. In Figure 8 dimensionless eigenfrequency of the $m = 3$ mode is plotted against dimensionless rotational frequency for three of the EOSs with various stiffness, with the gravitational mass of the model being fixed (as $M = 1.4M_\odot$). The EOS B is the softest among the three, and the EOS WFF3-NV, EOS L become stiffer

³With these coefficients introduced, our system of equations is free from coefficients that diverge at the stellar surface for relatively stiff EOS unlike those of MSB.

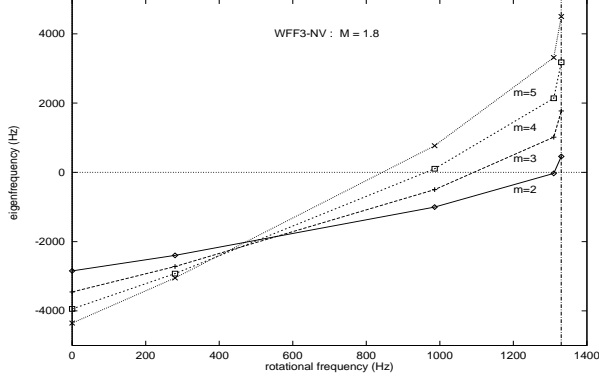


Fig. 1.— Eigenfrequencies of f-modes for the neutron stars constructed with the WFF3-NV EOS and $M = 1.8M_{\odot}$. It should be noted that both the eigenfrequency and the rotational frequency of the stars are not the angular frequencies but the ordinary frequencies. Symbols have the following meanings: ' \diamond ' for $m = 2$ mode, '+' for $m = 3$, ' \square ' for $m = 4$ and ' \times ' for $m = 5$. The vertical line in the right part is the maximum frequency which corresponds to the mass-shedding limit of the sequence.

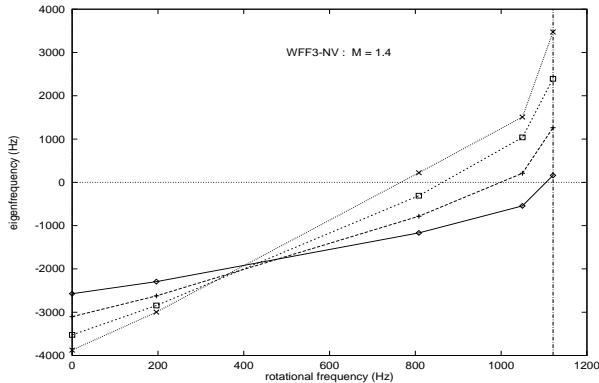


Fig. 2.— Same as Figure 1 except for $M = 1.4M_{\odot}$.

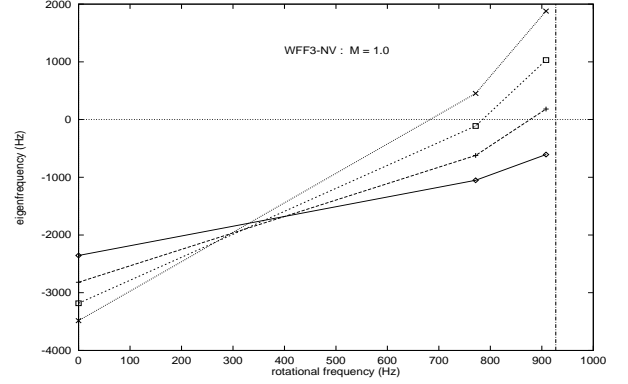


Fig. 3.— Same as Figure 1 except for $M = 1.0M_{\odot}$.

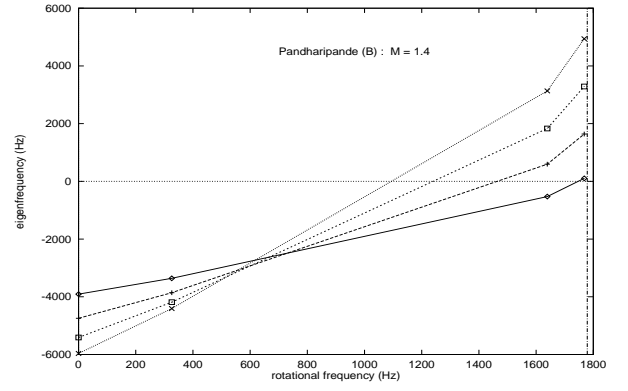


Fig. 4.— Same as Figure 1 except for the EOS B and $M = 1.4M_{\odot}$.

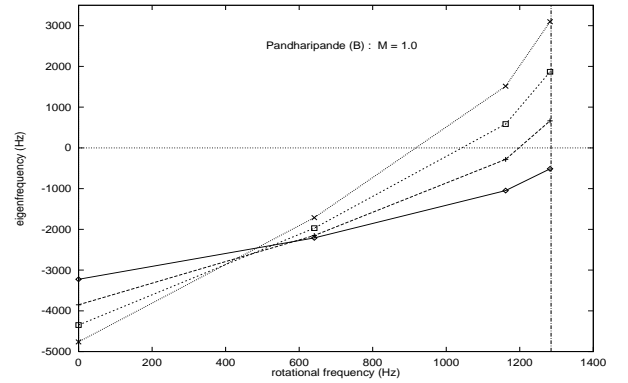


Fig. 5.— Same as Figure 4 except for $M = 1.0M_{\odot}$.

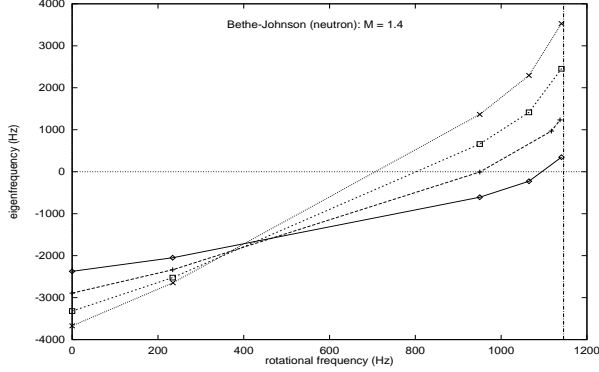


Fig. 6.— Same as Figure 4 except for the EOS Bethe-Johnson (neutron).

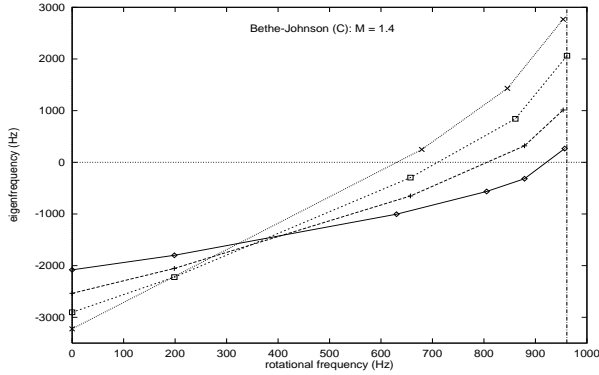


Fig. 7.— Same as Figure 4 except for the EOS C.

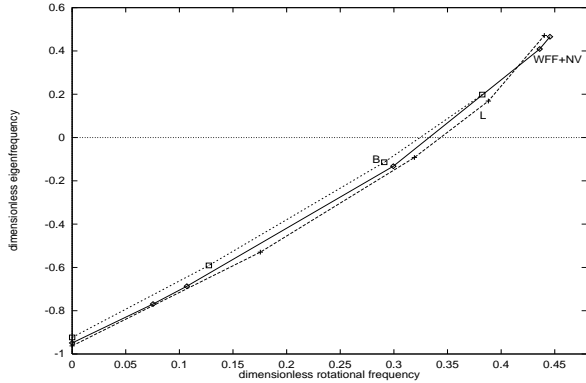


Fig. 8.— Dimensionless eigenfrequency of $m = 3$ mode is plotted against the dimensionless rotational frequency. The three sequences correspond to the same gravitational mass ($M = 1.4M_{\odot}$) models with different EOSs, WFF3-NV, B and L.

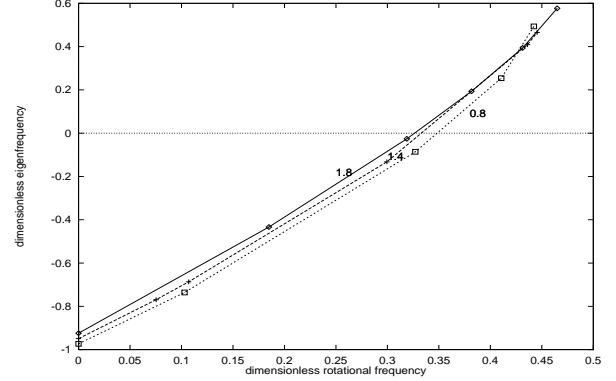


Fig. 9.— Same as Figure 8, except that the EOS is fixed (WFF3-NV) and the gravitational masses are varied ($M = 1.8, 1.4, 0.8M_{\odot}$).

in this order. Normalization factor of them is $\sqrt{4\pi\bar{\rho}}$, where $\bar{\rho} \equiv M/V_p$ is the averaged density with M and V_p being the gravitational mass and the proper volume of the equilibrium star. We can see that with this normalization the eigenfrequency is rather insensitive to the stiffness of the EOS from cases with no rotation to those nearly at the mass-shedding limits.

Figure 9 displays the variation of the normalized eigenfrequency due to the gravitational mass difference, with the EOS being fixed (as WFF3-NV). It is seen that increase in gravitational mass makes the mode frequency larger, which corresponds to the effect of the softening of the EOS in Figure 8. This is reasonable since the strong self-gravity of the star tends to induce its density profile to be concentrated to the central region of it, which effectively realizes the configuration with the softer EOS.

In Figures 10 and 11, we show the typical behavior of the eigenfunction q . The equilibrium models compared in these two figures have the same central density but the rotational frequencies are different. In both models, the function q increases monotonically from the center to the surface of the star along the radial spokes in the surface-fitted coordinate. For the slowly rotating model (Fig.10), the angular dependence of the q is nearly that of the associated Legendre function, $P_l^m(\cos\theta)$ (in this case $l = m = 4$), whereas rapid rotation tends to shift the distribution of the function q to the equatorial plane (Fig.11).

To see the 'radial' dependence of the eigenfunction, we show the function q on the equatorial plane (Fig.12). Here the same models are used as those

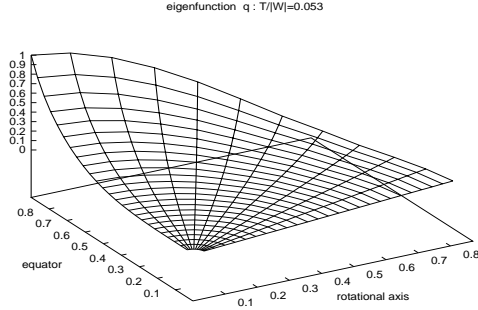


Fig. 10.— An example of the eigenfunction q (see text) for a slowly rotating star with the WFF3-NV EOS. A quarter of the meridional cross section of the star is shown. The mode number $m = 4$. The radial coordinate distance is normalized by using $c/(4\pi\epsilon_c)^{1/2}$ where c is the velocity of light and ϵ_c is the central mass density of the star. The amplitude of the eigenfunction is normalized such that the value of q at the surface point in the equatorial plane becomes unity. The parameters of the equilibrium model are: $\epsilon_c = 1.0 \times 10^{15} \text{g/cm}^3$, the rotational frequency $f = 285 \text{ Hz}$, $M = 1.19M_\odot$ and $T/|W| = 0.053$. The eigenfrequency $\nu = -2391 \text{ Hz}$.

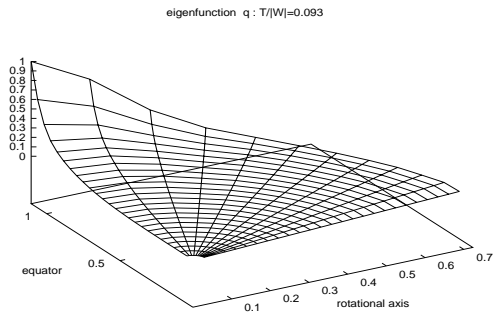


Fig. 11.— The eigenfunction q for a rapidly rotating star. The same mode as in Figure 10. The parameters of the equilibrium model are: $\epsilon_c = 1.0 \times 10^{15} \text{g/cm}^3$, $f = 1092 \text{ Hz}$, $M = 1.43M_\odot$ and $T/|W| = 0.093$. The eigenfrequency $\nu = 1250 \text{ Hz}$.

in Figures 10 and 11. As a 'radial' coordinate here we take the value $x \equiv 1 - \epsilon/\epsilon_c$, which roughly represents the matter-energy distribution of the equilibrium stars. As seen in this figure, the distribution of the function q is concentrated to the surface region as the star rotates more rapidly. In the Newtonian theory, the same situation seems to improve the Cowling approximation for rapidly rotating stars (Yoshida 1997) because the role of perturbed gravitational potential becomes less important. Roughly speaking, less part of the stellar mass participates in the oscillation as the star rotates more rapidly. This is also likely to be the case in general relativistic stars, though we have no 'exact' quasi-normal modes to compare with.

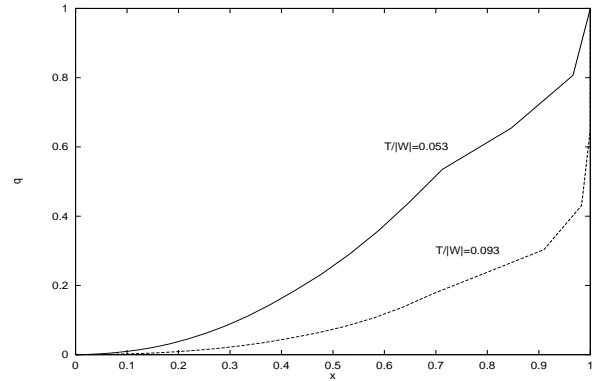


Fig. 12.— The eigenfunction q on the equatorial plane is plotted against the density coordinate x . The equilibrium models are the same as in Figure 10 and 11. Mode number $m = 4$. The solid curve is that for the model with $T/|W| = 0.053$, whereas the dashed one is that for the model with $T/|W| = 0.093$.

In Figure 13 the differences of radial behavior in the equatorial plane between modes with different m are shown. Here the radial coordinate is that of the surface-fitted coordinates. It can be seen that as m increases, the main part of oscillation of the star shifts outward where the amount of the mass fraction decreases. This can make the Cowling approximation more accurate for higher order modes (see Table 1).

3.2. Neutral Points of the CFS Instability

As is already remarked, we can estimate the neutral points of the CFS instability by finding zeroes of

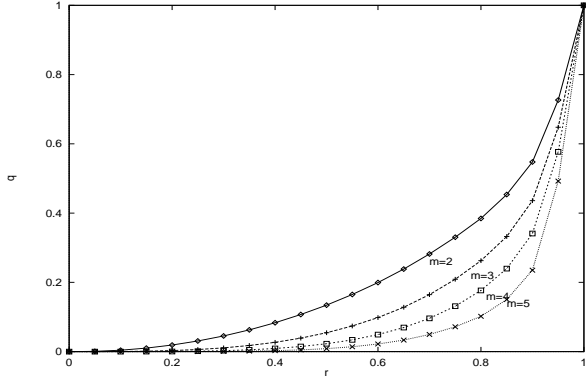


Fig. 13.— The eigenfunction q on the equatorial plane with different mode numbers. The radial coordinate distance is that of the surface-fitted coordinate. The equilibrium model is the same as that in Figure 11. Symbols have the same meanings as in Figure 1.

the eigenfrequencies.⁴ In Table 1 we compare the values of $T/|W|$ at the neutral points of the instability with those obtained by MSB. Here we summarize the tendency of the Cowling approximation in general relativity as follows: (1) for the same EOS and for the same mode number, the Cowling approximation gives better results as the central energy density of the model increases; (2) for the same equilibrium model, it results in more accurate values for larger mode numbers; and (3) the Cowling approximation has a tendency to overestimate the stability in the case of relatively weak gravity (cf. the Newtonian case in Yoshida 1997). These are qualitatively consistent with the previous results in YE. In contrast to the property (3), for larger central density (strong gravity) models, higher order modes seem to be underestimated in its stability by the Cowling approximation. As for the bar mode there seems no improvement with increase of the central density.

When the EOS is fixed, we can calculate an eigenfrequency of a mode for the model with a given rotational frequency f (Hz) and a given gravitational mass M (M_\odot). Then we have a neutral stability curve of the CFS instability for the mode in the $f - M$ plane as a set of zeroes of the eigenfrequencies. Four neutral stability curves corresponding to four different modes with different EOS are shown in Figures 14 – 17.

⁴Note that the neutral points here are *not* determined by using the graphs shown in the previous section. More detailed data sets have been used to obtain them.

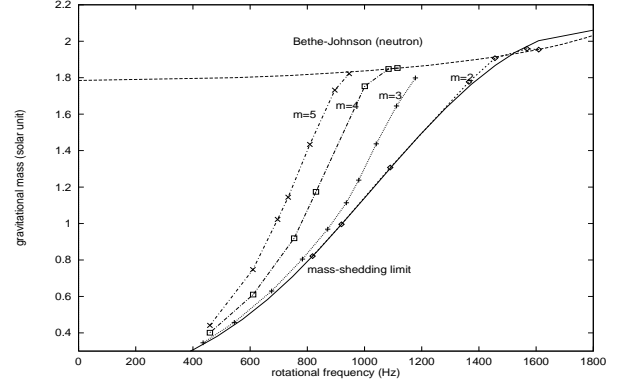


Fig. 14.— Neutral stability curves of the f-mode in the $f - M$ plane. The gravitational mass is normalized by the solar mass. The EOS is that of Bethe-Johnson without hyperon contribution. The solid line is the mass-shedding limit curve. The dashed line is the approximate maximum mass curve for a given rotational frequency (see text). Symbols used here are the same as in Figure 1.

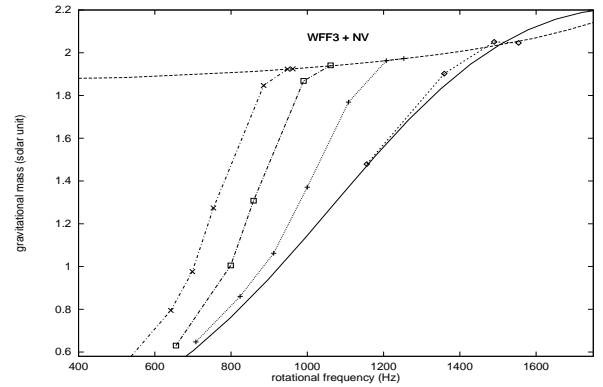


Fig. 15.— Same as Figure 14 except for the WFF3-NV EOS.

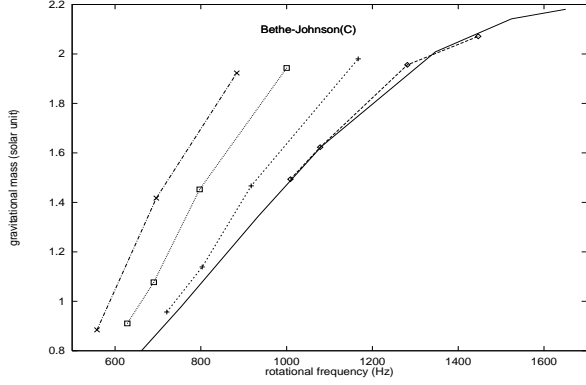


Fig. 16.— Same as Figure 14 except for the EOS C. The approximate maximum mass curve is omitted here.

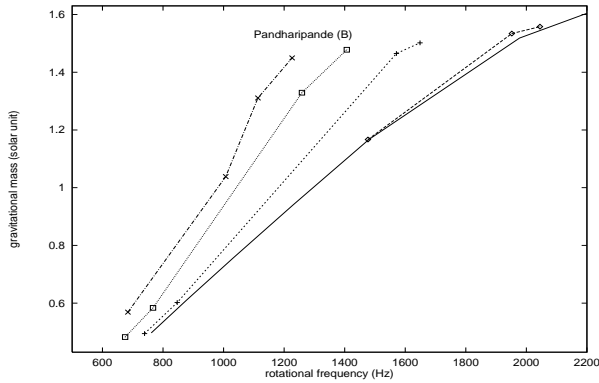


Fig. 17.— Same as Figure 14 except for the EOS B.

Table 1: Comparison of values of $T/|W|$ at neutral points with the results by Morsink et al. (1998)

| EOS | mode | $\epsilon_c (\times 10^{15} \text{g/cm}^3)$ | present | MSB |
|-----|---------|---|---------|-------|
| A | $m = 2$ | 1.0 | 0.094 | 0.082 |
| | | 3.2 | 0.079 | 0.056 |
| | $m = 3$ | 1.0 | 0.081 | 0.066 |
| | | 3.2 | 0.049 | 0.044 |
| | $m = 4$ | 1.0 | 0.056 | 0.054 |
| | | 3.2 | 0.035 | 0.035 |
| | $m = 5$ | 1.0 | 0.043 | 0.044 |
| | | 3.2 | 0.027 | 0.029 |
| C | $m = 2$ | 0.74 | — | 0.087 |
| | | 0.90 | 0.098 | 0.082 |
| | | 2.5 | 0.077 | 0.059 |
| | $m = 3$ | 0.70 | 0.076 | 0.066 |
| | | 0.95 | 0.071 | 0.061 |
| | | 2.5 | 0.048 | 0.046 |
| | $m = 4$ | 0.70 | 0.053 | 0.052 |
| | | 1.0 | 0.049 | 0.047 |
| | | 2.5 | 0.035 | 0.036 |
| | $m = 5$ | 1.0 | 0.036 | 0.038 |
| | | 2.5 | 0.027 | 0.028 |

Figure 14 displays those for the EOS of Bethe-Johnson without hyperon. The region of the left hand side of each curve is the stable region against the CFS mechanism for the corresponding mode. The solid line is the mass-shedding limit curve on which the gas on the surface in the equatorial plane rotates with the local Keplerian velocity. The dashed line in the upper region is the approximate maximum mass line for a given rotational frequency. The reason why we use the word 'approximate' is that to obtain it we do not constrain the rotational frequency to be constant but the axis ratio of the configuration to be constant (Komatsu et al. 1989).

At first sight, it seems strange that for sufficiently rapidly rotating cases we have a model in the right hand side region of the mass-shedding curve. It seems to imply that for a given mass we have equilibrium models that have larger rotational frequencies than the mass-shedding case. This comes from the fact that the rotational frequency f is *not* a proper measure of the rotation for extremely rapidly rotating stars (see appendix for its explanation).

4. Applications

We here apply our results to two issues of interest in neutron star physics. One is the estimation of the time scale of the CFS instability. The other is related to the resonant excitation of f-modes in inspiraling compact binary systems which are possible targets of the gravitational wave detectors under construction.

4.1. CFS Instability of Neutron Stars

In the previous section neutral points of the CFS instability are determined. Then what we want to know next is *how fast these unstable perturbations grow beyond these points*. Unfortunately our approximation does not provide us the answer directly. What is expected to happen in the real process is that the stellar free oscillations with non-zero frequencies couple to gravitational wave radiation which carries its energy to infinity, and the frequencies inevitably have imaginary parts. This is the problem of the so-called *quasi-normal mode* which is well-known in black hole physics. To obtain complex eigenfrequencies, we must take the metric perturbations into account and the *out-going wave* conditions must be specified to them. This task is extraordinarily difficult for rapidly rotating stars and no investigation has been accomplished for it yet.

As its alternative, there have been several works which estimates the growth time of the instability by applying the gravitational radiation reaction potential of the post-Newtonian expansion (Thorne 1969) to Newtonian stellar oscillations. In this approximation, we only need to know the time dependency of the mass multipole of the oscillating star.

Here we roughly estimate the growth rates of the instability by following Comins (1979), who investigated the secular effects of the gravitational radiation reaction and viscosity on the oscillating Maclaurin spheroids.

According to the analysis of Comins, the effect of gravitational radiation adds a small imaginary part to the oscillation frequency viewed from the co-rotating frame with the star $\Sigma \equiv -2\pi(\nu - f)$ as follows:

$$\delta\Sigma = \frac{2iG \left[\frac{M}{\frac{4}{3}\pi R_1^3} \right] (m+1)(m+2)R_1^{2m+1} (2\pi)^{2m} \nu^{2m+1}}{(m-1) [(2m+1)!!]^2 [(m-1)f - \nu] c^{2m+1}}, \quad (2)$$

where c and G are the velocity of light and the gravitational constant, respectively, and R_1 is the equa-

torial radius of the star. From this expression, we can estimate the e-folding time τ_{GR} for the growth of perturbations as follows:

$$\tau_{GR}(\text{sec}) = k(m) \left[(m-1) \left(\frac{f}{\text{kHz}} \right) - \left(\frac{\nu}{\text{kHz}} \right) \right] \times \left(\frac{M}{M_\odot} \right)^{-1} \left(\frac{R_1}{10\text{km}} \right)^{-2m+2} \left(\frac{\nu}{\text{kHz}} \right)^{-2m-1} \quad (3)$$

where $k(m)$ is defined as,

$$k(m) = \frac{10^{2m-4} [c/10^{10}]^{2m+1} (m-1) [(2m+1)!!]^2}{4(2\pi)^{2m-1} (m+1)(m+2)}. \quad (4)$$

This formula is applied to the neutron star models of $M = 1.4M_\odot$ with the WFF3-NV EOS (Table 2).

It is seen that, as the rotation rate is increased, the lower order modes suffer stronger destabilization effect by gravitational radiation, which originates from the efficiency of gravitational radiation of these lower order oscillations, than the higher order modes whose neutral points reside at the lower rotational frequencies. As a result these modes shown here have the same order of timescale near the mass-shedding limit.

Table 2: Estimated timescale in units of second of the CFS instability for the $M = 1.4M_\odot$ star with the WFF3-NV EOS.

| $f(\text{Hz})$ | $m = 3$ | $m = 4$ | $m = 5$ |
|----------------|--------------------|-----------------|--------------------|
| 818 | — | — | 9×10^{15} |
| 952 | — | — | 2×10^9 |
| 1006 | 4×10^{19} | 4×10^7 | 6×10^7 |
| 1053 | 3×10^7 | 1×10^6 | 3×10^6 |
| 1117 | 1×10^3 | 1×10^3 | 3×10^3 |

This estimation needs to be treated as very rough one because we assume that the formulae for Newtonian Maclaurin spheroids are applicable to the relativistic neutron star models and because the correspondence of equilibrium quantities such as the mass and the equatorial radius is vague. However, qualitative behavior of the modes would be the same even if more refined treatment would be employed.

4.2. Resonant Excitation of the f-modes for Inspiring Compact Binary Systems

Inspiring compact binary systems (neutron star–neutron star (NS/NS), black hole–neutron star (BH/NS) and black hole–black hole) are the most promising sources of gravitational wave for large interferometry gravitational wave detectors under construction such as LIGO and VIRGO (see e.g. Thorne 1994 and the references therein). These detectors will be able to observe the inspiring phase where components of the system are well approximated by the point masses. To extract meaningful results from the gravitational wave signals, it is indispensable to have sufficiently accurate theoretical templates of wave forms in the frequency range of $10 - 10^3$ Hz to which these detectors are sensitive (Cutler et al. 1993).

In this context, if at least one of the components is a neutron star, its internal hydrodynamical degrees of freedom may be a potential threat to the template construction. Bildsten & Cutler (1992) examined the problem of the ‘equilibrium tide’ and the issue of the tidal locking of the components. The tidal locking which causes synchronization of the spin and the orbital motion seems rather unlikely to occur according to their result, and the theoretical template suffers only a negligible correction by it. Excitations of stellar oscillations of the inspiring stars, or the ‘dynamical tide’, is another issue to be considered. Reisenegger & Goldreich (1994) and Lai (1994) investigated resonant excitations of g-modes and their effects on the inspiral orbit. For slowly rotating stars g-modes frequencies may fall in the range as low as the orbital resonant frequency. According to their results, however, g-modes affect the orbit negligibly, since the coupling between tidal potential and g-mode eigenfunctions is rather weak.

As we have seen, counter-rotating f-modes of neutron stars pass the neutral points viewed from the asymptotic inertial frame if the star rotates sufficiently rapidly. Thus it may suffer resonant excitations during the inspiral phase.⁵ Once the resonance condition is fulfilled, the f-mode is likely to be a much more dangerous obstacle to the construction of the

theoretical template, since the f-mode eigenfunction couples more strongly with the tidal potential. We here adopt the simple oscillator model by Reisenegger & Goldreich (1994) and examine the effect of the mode excitation.

A sinusoidal external force operating on a star with a mass M_1 whose frequency fulfills the resonance condition, $\nu/m = n_{\text{orb}}$, where n_{orb} is the orbital frequency, excites a mode whose energy amounts to,

$$\varepsilon = \frac{(F\delta t)^2}{8M_1}, \quad (5)$$

during the resonance time interval δt , which is typically the decay time of the orbit by gravitational radiation. The external tidal force by the companion with a mass M_2 is estimated by the following formula:

$$F = \frac{GM_1M_2}{R_1^2} \left(\frac{R_1}{a} \right)^{m+1} S, \quad (6)$$

where R_1 is the stellar radius and a is the separation of the binary system. The factor S is the ‘overlap integral’ describing the efficiency of the tidal force on an eigenfunction defined by

$$S = \int_{M_1} \sqrt{-g} u^t dr d\theta d\varphi \left(\frac{\epsilon}{c^2} \right) \vec{\xi} \cdot \vec{P}, \quad (7)$$

where g is the determinant of the metric of the background spacetime, u^t the time component of the 4-velocity of the unperturbed stellar fluid, $\vec{\xi}$ is the Lagrangian displacement and $\vec{P} = \nabla(r^m Y_m^m(\theta, \varphi))$.

The vibrational energy of an excited mode ε is compared with the orbital energy decrease by gravitational radiation ΔE in the time interval δt ,

$$\frac{\varepsilon}{\Delta E} = \alpha_m [M_2/M_1; R_1] \left(\frac{n_{\text{orb}}}{100\text{Hz}} \right)^{\frac{8m-23}{6}} S^2, \quad (8)$$

where the factor α_m depends on the mode number, the mass ratio of the components and the stellar radius. If this ratio is not negligible compared with unity, the assumption that the binary orbit evolves solely by gravitational radiation from the orbital motion should be amended. If the stellar radius and the mass ratio of the components are assumed to be $R_1 = 10\text{km}$ and $M_2/M_1 = 1$, the factors α_m are computed as follows:

$$\alpha_m = \begin{cases} 5 \times 10^1 & (m=2) \\ 0.4 & (m=3) \\ 0.004 & (m=4) \\ 3 \times 10^{-5} & (m=5) \end{cases}. \quad (9)$$

⁵As seen in Bildsten & Cutler, the tidal synchronization of inspiring components is unexpected. So the initial angular velocities of both components are preserved during the inspiral. We here consider the case in which at least one neutron star in the system has a sufficient angular velocity to suffer the orbital resonance. Whether such systems do exist actually or not is beyond our discussion here.

If the mass ratio is larger, say $M_2/M_1 = 10$ (BH/NS case), they are:

$$\alpha_m = \begin{cases} 2 & (m=2) \\ 6 \times 10^{-3} & (m=3) \\ 2 \times 10^{-5} & (m=4) \\ 5 \times 10^{-8} & (m=5) \end{cases} . \quad (10)$$

The overlap integral S may be computed by using the eigenfunction of the mode obtained by the Cowling approximation. We find that $S \simeq 1$ for the bar mode and S is larger than 0.6, 0.3, and 0.2 for $m = 3, 4$, and 5 modes, respectively, for all the models from the non-rotating state to the mass-shedding limit.⁶

4.2.1. Neutron Stars with the Prograde Rotation to the Orbital Motion

When the star under consideration rotates in the same direction as its orbital motion, the resonance condition of 'counter-rotating' modes and the orbital motion may be fulfilled for the states beyond the neutral points of the modes. In this case, the bar mode may not be significant except for the stars which rotate with velocities of nearly the mass-shedding limit.

As seen from Figs. 1 – 3, for higher order modes, the orbital frequencies at the resonances, $n_{\text{orb}} = \nu/m$, may be under 10^3Hz for the realistic EOS⁷, even at the mass-shedding limit of the star. Using the formula of $\varepsilon/\Delta E$ above, it is observed that the higher modes than $m = 4$ may not affect the orbital evolution governed by gravitational radiation during the inspiral phase which will be observed by the gravitational wave antennas like LIGO/VIRGO. It is also seen that for systems with a large mass ratio like a BH/NS binary, the energy deposited in the NS vibration is too small to affect the binary orbit.

As for the $m = 3$ mode, its excitation may affect the stability and the evolution of the system if the star has a sufficiently large rotational frequency (for example, larger than 850Hz for $M = 1.0M_\odot$; larger than 1000Hz for $M = 1.4M_\odot$), since the vibrational energy is no more negligible compared with

the gravitational radiation energy loss from the system. Moreover n_{orb} at its resonance is in the range of sensitivity of LIGO/VIRGO detectors, the excitation may be observed as the discrepancy of the signal from its theoretical template.

4.2.2. Neutron Stars with the Retrograde Rotation to the Orbital Motion

If the star rotates in the retrograde direction against its orbital motion, the resonance condition of the modes and the orbit requires the rotational frequency of the star to be lower than that of the neutral points. Thus the resonance condition can drop to the frequency range of LIGO/VIRGO sensitivity windows even for lower m modes.

Significant is the fact that the bar mode which couples most strongly to the tidal potential can be resonant for a wide range of rotational frequency of the star. For $M = 1.4M_\odot$ models, stars with rotational frequency above 400Hz may suffer the resonant excitation on its inspiraling path in the gravitational wave antennas' sensitivity window (for $M = 1.0M_\odot$ case, this frequency may go down to 200Hz). The factor α_2 amounts to 50 for an equal mass NS/NS binary, and to 2 even in BH/NS cases with the mass ratio $M_2/M_1 = 10$. Since the overlap integral $S \sim 1$ for the bar mode, the resonant excitation would affect the evolution of the binary orbit significantly.

Moreover the $m = 3$ mode can be excited in the stars rotating with frequency as low as 20Hz (for $1.4M_\odot$ case). Thus theoretical templates of gravitational wave signals from compact binary systems containing NS with retrograde rotation should almost always take the resonant excitation of the counter-rotating f-modes into account.

SY would like to thank Prof. B. Schutz and Dr. C. Cutler for their warm and generous hospitality at Max-Planck-Institut für Gravitationsphysik (Albert-Einstein-Institut) in Potsdam where a part of the numerical computation was done and this paper was prepared. The authors are also grateful to the anonymous referee for useful suggestions.

REFERENCES

- Andersson, N. 1998, *ApJ*, 502, 708
Andersson, N., Kokkotas, K., & Schutz, B. F. 1998, *ApJ*, Submitted. (Preprint: astro-ph/9805225)

⁶Here we made rough an estimation which assumes the validity of Newtonian and slow-rotation-limit formulae used in the Reisenegger & Goldreich in our investigation. It is intended only to display that the overlap integral should be nearly order of unity in the low order mode cases.

⁷Here we pay attention only to the models with the WFF3-NV EOS.

Arnett, W. D., & Bowers, R. L. 1977, *ApJS*, 33, 415

Baumgart, D., & Friedman, J. L. 1986, *Proc. R. Soc. Lond.*, A405, 65

Bethe, H. A., & Johnson, M. 1974, *Nucl. Phys.*, A230, 1

Bildsten, L., & Cutler, C. 1992, *ApJ*, 400, 175

Chandrasekhar, S. 1970, *Phys. Rev. Lett.*, 24, 611

Comins, N. 1979, *MNRAS*, 189, 255

Cutler, C. et al. 1993, *Phys. Rev. Lett.*, 70, 2984

Friedman, J. L. 1978, *Comm. Math. Phys.*, 62, 247

Friedman, J. L., & Schutz, B. F. 1978, *ApJ*, 222, 281

Komatsu, H., Eriguchi, Y., & Hachisu, I. 1989, *MNRAS*, 239, 153

Lai, D. 1994, *MNRAS*, 270, 611

Lindblom, L. 1986, *ApJ*, 303, 146

Lindblom, L., Owen, B. J., & Morsink, S. M. 1998, *Phys. Rev. Lett.*, 80, 4843

Morsink, S. M., Stergioulas, N., & Blattnig, S. R. 1998, *ApJ*, Submitted. (Preprint: gr-qc/9806008)

Nozawa, T., Stergioulas, N., Gourgoulhon, E., & Eriguchi, Y. 1998, *A&A*, in press.

Negele, J. W., & Vautherin, D. 1973, *Nucl. Phys.*, A207, 298

Reisenegger, A., & Goldreich, P. 1994, *ApJ*, 426, 688

Stergioulas, N., & Friedman, J. L. 1997, *ApJ*, 492, 301

Thorne, K. S. 1969, *ApJ*, 158, 997

Thorne, K. S. 1994, in *Relativistic Cosmology*, ed. M. Sasaki (Tokyo:Universal Academy Press), 67

Wiringa, R. B., Fiks, V., & Fabrocini, A. 1988, *Phys. Rev.*, C38, 1010

Yoshida, S. 1997, Ph.D. thesis, University of Tokyo

Yoshida, S., & Eriguchi, Y. 1997, *ApJ*, 490, 779

A. Equilibrium Models with Lower Masses than the Mass-Shedding Limit Mass

In Figures 14 and 15 we see a strange behavior of the rapidly rotating equilibrium models, i.e., the existence of equilibrium models in the right part of the figure divided by the mass-shedding curve. It originates from the fact that the rotational frequency becomes an improper index for the stellar rotation for sufficiently rapid rotation models.

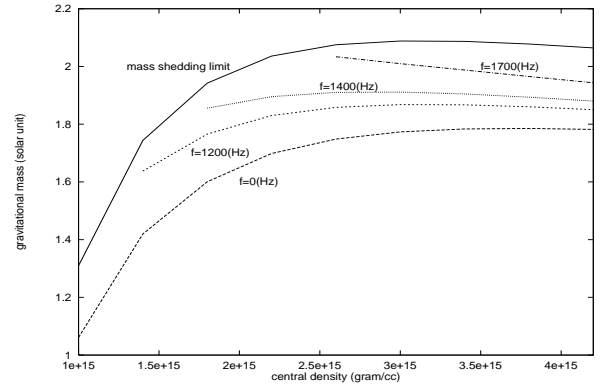


Fig. A18.— The constant-rotational-frequency curves in the central density – gravitational mass plane. Here the models are constructed with the EOS Bethe-Johnson (neutron).

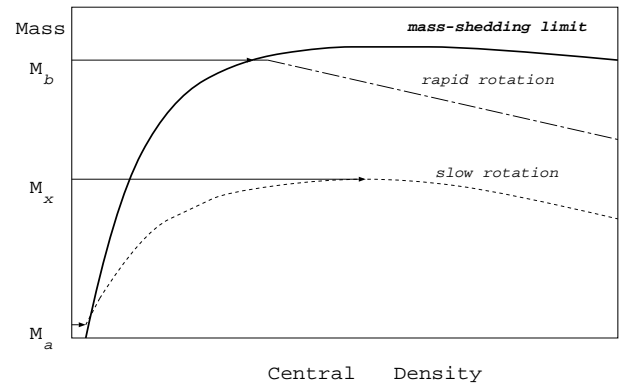


Fig. A19.— Schematic figure of constant-rotational-frequency curves. The solid line is the mass-shedding curve. The dotted and dot-short-dashed lines respectively corresponds to the constant-rotational-frequency curves with slow and rapid rotation.

To see this we should know how gravitational mass changes with the central density of the star (Figure 18, Figure 19). In Figure 18 gravitational mass M

This 2-column preprint was prepared with the AAS L^AT_EX macros v4.0.

of the equilibrium models with the same angular frequency is shown as a function of the central energy density. The solid line is the mass-shedding curve below which equilibrium models can be allowed to exist. Figure 19 is a schematic abstraction of the situation in Figure 18.

While the angular velocity is small the curve with a constant rotational frequency f has a maximum in the allowed region, thus the mass of the mass-shedding configuration M_a in Figure 19 is *smaller* than the maximum mass M_x for this value of angular frequency ($M_a \leq M \leq M_x$). However, for the case with sufficiently rapidly rotation, the curve with constant angular frequency shows monotonically decreasing behavior with no local maximum in the allowed region. In this case, the gravitational mass at the mass-shedding model M_b is *larger* than that of other equilibrium models with the same rotational frequency ($M_b \geq M$). This situation corresponds to the existence of the equilibrium model with smaller M than the mass-shedding limit in Figures 14 and 15.